Supporting Information

Fabrication of MIL-53(Fe)/Ag_3PO_4 cooperated Photoreduction of Ag^0 Particles with outstanding Efficiency on photo-driven H_2 Evolution and Pollutant Degradation

Hao Zeng, Jungang Yi, Linfeng Zhang[1, 3*], Huadong Wu[1], Kun Wu[1, 2], Jia Guo[1*]

1 Key Laboratory for Green Chemical Process of Ministry of Education, Hubei Key Laboratory of Novel Reactor and Green Chemical Technology, School of Chemical Engineering and Pharmacy, Wuhan Institute of Technology, Wuhan 430205, People's Republic of China

2 The College of Post and Telecommunication of Wuhan Institute of Technology, Wuhan 430073, People's Republic of China

3 School of Chemical Engineering and Technology, Tianjin University, Tianjin 300072, PR China

***Corresponding authors:** L. Zhang: E-mail: lfzhang@wit.edu.cn, Fax number: +86 027-87905262; J. Guo: E-mail: guojia@wit.edu.cn, Fax number: +86 027-87194980

2.1 Chemicals

Terephthalic acid (H_2-BDC), Triethanolamine (TEOA) and Eosin (alcohol soluble, EY) were purchased from Aladdin. Iron (III) chloride hexahydrate ($FeCl_3 \cdot 6H_2O$), disodium hydrogen phosphate ($Na_2HPO_4 \cdot 12H_2O$), silver nitrate ($AgNO_3$), Methanol (MOH), N, N-dimethyl-formamide (DMF) were all purchased from Sinopharm Chemical Reagent Co., Ltd (China). All of the chemicals were commercially available analytical grade and used without further purification.

2.2 Preparation of MFAA composites

2.2.1 Preparation of MIL-53(Fe)

MIL-53(Fe) was synthesized based on a previous report [1]. Typically, a mixture of H_2-BDC (2 mmol, 0.49 g), $FeCl_3 \cdot 6H_2O$ (2 mmol, 0.81 g) and 42 mL DMF was vigorously stirred at room temperature for 1 h. Then, the mixed solution was transferred to a 100 mL Teflon-lined autoclave and then was heated at 150 °C for 6 h. After cooling to ambient temperature, the suspension was suction filtration and washed with ethanol. To completely remove the residue, the product was heated at 150 °C for 12 h again.

2.2.2 Preparation of Ag/Ag_3PO_4 composites

The appropriate amount of $AgNO_3$ was dissolved in deionized water to obtain 0. 1mol/l silver nitrate solution; Next, a certain proportion of $Na_2HPO_4 \cdot 12H_2O$ solution was added dropwise to the mixed solution. Finally, the mixture was stirred in the dark for 12 h and filtered to obtain the Ag_3PO_4 sediment. After that, the 0.01g Ag_3PO_4 was dispersed in 30 mL methanol solution and placed under a UV-Vis light for a certain period to reduce part of Ag^+ to Ag^0. The lighting time was designed as 1, 5, and 10 min, respectively.

2.2.3 Preparation of MIL-53(Fe)/Ag/Ag_3PO_4 (MFAA) composites

In order to obtain the MIL-53(Fe)/Ag/Ag_3PO_4 composites, firstly, 0.1 g of MIL-53(Fe) was dispersed in 50 mL of absolute ethyl alcohol and stirred vigorously for 10 min; Then, the different lighting times of Ag/Ag_3PO_4 obtained already were separately added into the above solution. Finally, the mixture was placed in the dark and stirred until the solvent volatilizes completely. Then, the resulting MIL-53(Fe)/Ag/Ag_3PO_4 composites were defined as $MFAA_x$ (x=10.1, 10.5, 10.10) or MFA(x=0).

2.3 Characterization of the as-prepared MIL-53(Fe)/Ag/Ag_3PO_4 composites

The morphology of the composites was analyzed by a Zeiss Merlin compact field emission scanning electron microscope (FESEM) and Merlin compact-61-78 with an acceleration voltage of 10 kV. The elemental mapping of $MFAA_{10.5}$ was received by the EDX coupled to FESEM. The high-resolution transmission electron microscopy (TecnaiG2 F20 S-TWIN, FEI, USA) was used to get HRTEM images. Fourier transform infrared (FT-IR) spectroscopy (NICOLET 5700, USA) was applied to investigate the functional groups on the samples. The crystal structures of the samples were investigated by X-ray diffraction (XRD, Bruker D8 Advance, Germany), which used Cu-Kα (λ=0.15418 nm) and scanned angle range from 5 to 60°. The UV-vis diffuse reflectance spectra (UV-vis DRS) of the prepared samples were obtained on a UV-Vis spectrophotometer (U-3900, Japan), and $BaSO_4$ was chosen as a reflectance standard. The surface elemental composition was performed via X-ray photoelectron spectroscopy (XPS, Escalab 250XI, Thermo Fisher, USA). The photoluminescence (PL) spectra and the time-resolved PL spectrum of the materials were analyzed on a fluorescence spectrometer (F-4600 FL, Japan) with an excitation wavelength at 375 nm, which the scanned angle ranged from 200 to 800 nm. The intermediates of CIP photodegradation were detected by an LTQ XL (USA, Thermo Electron) LC-MS instrument. Photoelectrochemical

measurements include photocurrent, electrochemical impedance spectroscopy (EIS), and Mott–Schottky curves. The ion leaching during the photoreaction was detected by ICP-MS (Agilent 7700). The EIS measurement was performed in a homemade three-electrode quartz cell employing electrolyte solution (the concentration of $K_3Fe(CN)_6$, $K_4Fe(CN)_6$, and KCl were all 0.1M). The photocurrent and Mott–Schottky curves were performed in a homemade three-electrode quartz cell employing 0.2 M Na_2SO_4 as electrolyte solution and using a CHI 600 electrochemical workstation (Shanghai, China), the difference was using a 300 W xenon lamp (PLS-SXE 300) as the light source for the photocurrent. DFT calculation method is used to study the interface charge transfer mode and enhancement mechanism, all spin-polarized calculations were performed using Vienna ab initio Simulation Package (VASP). The Perdew-Burke-Enrzerhof (PBE) parametrization of the generalized gradient approximation (GGA) was used to describe the electronic exchange-correlation energies. The criterion of total energy convergence in the optimization of the atomic structure is 10^{-5} eV, the convergence criterion of the atomic force is 0.05 eV/Å, and the cut-off energy of plane wave expansion is 400 eV. The Brillouin zone was sampled using the Monkhorst-Pack method with 2×2×1 k-point meshes. A vacuum layer of 15 Å was used along the c direction normal to the surface to avoid periodic interaction.

2.4 Photocatalytic performance assessment of composites

The photocatalytic performance of the composites was evaluated via the H_2 evolution under visible light irradiation. The experiment was performed in a 150 mL quartz reactor with a room temperature condensing system. And a 300 W Xenon lamp was employed as the visible light source, which was equipped with an ultraviolet cut-off filter. Typically, 20 mg of catalysts and quantitative EY and TEOA were dispersed in 90 mL of deionized water and durned in a vacuum for 30 min to

remove air. Then the high-efficiency hydrogenation (HER) system was turned on after the gas chromatography collection system was reached into a nitrogen atmosphere. The volume of hydrogen was collected and analyzed every 30 min by gas chromatography. The whole hydrogen evolution process was controlled at 4 h and the accumulative hydrogen yield was recorded.

Additionally, the pollutant degradation efficiency of the as-prepared composites was also evaluated under visible-light irradiation, using the 300 W Xe lamp with a 420 nm cut-off filter as the simulated light source. The ciprofloxacin (CIP) molecule was selected as the typical simulated pollutants. Specifically, 50 mL of the CIP solution (10 mg/L) was placed into a quartz glass reactor and then 10 mg of catalysts were added to the above solution. The mixture was placed in a dark environment and stirred for 60 min to reach the adsorption-desorption equilibrium. Then 2 mL of the supernatant was extracted for the measurement of the concentration every 10 min. The concentration of pollutants was determined via the absorbance using a PerkinElmer Lambda 35 spectrophotometer with the measuring wavelength decided at 272 nm.

The reusability and stability of the as-prepared $MAFF_{10.5}$ composites were estimated through cyclic experiments. Firstly, after the first cyclic degradation experiment was finished, then the composites were collected by centrifugation and drying. The dried composites were then used for another identical photocatalytic degradation experiment. Six cyclic degradation experiments were carried out with the composites under the same condition and then the recovered catalyst was collected for structural characterization. Similarly, the same cyclic operation was also implemented in the photocatalytic hydrogen production experiment. Subsequently, the reaction solution after cyclic degradation was tested by the O-phenanthroline-Fe spectrophotometer method, ammonium iron sulfate titration and ICP-MS characterization to investigate ion leaching [2].

After six cyclic degradation experiments, the used photocatalyst was collected by filtration. In the typical regeneration process, the 15 mL 0.05 M $NaNH_4HPO_4 \bullet 4H_2O$ was prepared as the reaction solution. Subsequently, after dispersing the used photocatalyst into the solution, 5 mL 15% H_2O_2 was added slowly for ensuring the complete reaction. The resulting product was collected by filtration and then exposed to UV-vis light again for 5 min for reduced Ag^0. Finally, the regenerated photocatalyst was applied to photodegrade the CIP solution.

2.5 Exploration of active radical

As for exploring the possible mechanism, the isopropanol (IPA), ethylenediamine tetraacetic acid disodium (EDTA-2Na), and p-benzoquinone (BQ) were chosen as different kinds of active specie scavengers were added to eliminate the specific active radical action while carrying on the photo-degradation reaction. Furthermore, the ESR characterization was also applied to distinguish the active radicals in the reaction solution on JES-FA200 (JEOL).

3.2 X-ray diffraction (XRD) and FT-IR spectra

As for FT-IR spectra exhibited in Fig. S1, all of the characteristic absorption peaks at 3700-2800 cm^{-1} can be attributed to the vibration of O-H. For the pure MIL-53(Fe), five absorption peaks could be observed at 1651, 1596, 1391, 748 and 547 cm^{-1}, respectively. Specifically, the absorption peak at 1651 cm^{-1} could attribute to the C=O stretching, which may be because of the incomplete conversion of DMF [3]. While the two peaks at 1596 and 1391 cm^{-1} can be attributed to the asymmetric and symmetrical vibration of the carboxyl group, which may be suitable evidence for the existence of the dicarboxylic acid linker in the MIL-53(Fe) structure. The two peaks at 748 and 547 cm^{-1} could attribute to the C–H bending vibration of the benzene ring and stretching vibration of Fe-O bonds, respectively. For the pure Ag_3PO_4, three absorption peaks could be observed at 1656,

999 and 557 cm^{-1}, respectively. The absorption peak at 1656 cm^{-1} could attribute to the stretching vibration of O-H inbound water, and the other two peaks at 999 and 557 cm^{-1} could attribute to the stretching vibration of P-O in phosphate. For the Ag/Ag_3PO_4 composites, the absorption peaks do not show any shifting compared with the pure Ag_3PO_4. Only the intensity of absorption peaks decreased, which was mainly due to the reduction of part of Ag^+. For the $MFAA_{10.5}$ composites, the absorption peaks are similar to the MIL-53(Fe). But the intensity of the absorption peak located at around 1600 cm^{-1} is increased, which may be attributed to the overlapping effect of the asymmetric vibration of the carboxyl group of MIL-53(Fe) and the stretching vibration of O-H inbound water of Ag_3PO_4. In addition, the intensity of series absorption peaks at around 1000 cm^{-1} is also increased, which is mainly due to the stretching vibration of P-O in phosphate.

3.5 Brumaire–Emmett–Teller (BET)

The photocatalytic activity is closely related to the specific surface area of composites because the large specific surface area can provide abundant active sites. **Fig. S2** showed the N_2 adsorption-desorption isotherms and the corresponding pore size distribution plots of the MIL-53(Fe) and $MFAA_{10.x}$ composites. As shown in **Fig. S2**, all of the composites exhibited a representative Langmuir type IV isotherm with an obvious hysteresis loop. From the change of specific surface area, it can be inferred that in the process of composite formation, Ag_3PO_4 with the extremely low specific surface area covered the surface of MIL-53(Fe), resulting in a sharp decrease of specific surface area ($MFAA_{10.1}$). However, as part of Ag^+ is reduced to Ag^0, the surface properties of the original MIL-53(Fe) are revealed. In addition, the introduction of Ag may remove DMF from MIL-53(Fe) [4]. As a result, the specific surface of $MFAA_{10.5}$ increase a little compared with MIL-53(Fe). Finally, with the excessive reduction of Ag^+, the surface pore diameter of MIL was blocked by the

aggregation of a large amount of silver, and the specific surface area and average pore diameter of $MFAA_{10.10}$ decreased again. The change in the specific surface area of the composite is also reflected in the adsorption test in photocatalytic degradation of CIP.

3.8 Photocatalytic activity for H_2 production and pollutant degradation

The exploration of the transition state and intermediary of pollutants in the photocatalytic degradation process are also important links in the research mechanism, to which liquid chromatography-mass spectrometry (LC-MS) was applied. As a result, the intermediates with the m/z identified 245, 263, 306, 334 and 362 were detected. On the basis of reported research, the most suitable explanation of the undergoing pathway in CIP degradation is piperazine oxidation which is shown in **Fig. S5** [5].

In the typical degradation pathway, the piperazine belonging to CIP was oxidated by $\bullet O_2^-$ and h^+, leading to the intermediate identified as A with m/z=362. Then the further oxidized intermediate D (m/z=306) was obtained due to the eliminated -CO groups of intermediates B (m/z=334) and C (m/z=334). Subsequently, the intermediate E was detected resulting from the removal of $-NH_2$ groups. However, the absent signal of the intermediate F may be because of the rapid transfer of F to G. Lastly, the final product G (m/z=245) was obtained by the defluorination.

3.9 Stability and reusability

In view of the oxidation-reduction reaction in the photocatalytic process, the leaching of Fe ions and Ag ions is also one of the criteria to measure the stability of the catalyst. For Fe ions, the O-phenanthroline-Fe spectrophotometer method was used to test the concentration of total Fe ions in the reaction solution which is exhibited in **Fig. S6a**. As presented, the catalyst remained stable during the adsorption process. Subsequently, the ion leaching of total Fe ions reached 0.104 mg/L

after 120 min photoreaction. That is to say, only 0.0052 mg total Fe ions were leached during the reaction which is almost negligible for 10 mg photocatalysts revolved in the reaction. Besides, the content of silver ions in the reaction solution was measured by ammonium iron sulfate titration. As a result, there is no sediment formation. Finally, the solution after photoreaction was measured by ICP-MS for reconfirming the content of total Fe and Ag ions. The result is that the content of the total Fe ions and Ag ions was identified separately as 0.185 mg/L and 0.089 mg/L, which means there were only 0.00925 mg Fe and 0.0044 mg Ag leaching during the reaction. In conclusion, ion leaching in the reaction process is almost negligible, which will not affect the repeatability of the catalyst.

The regeneration of silver-containing photocatalysts also means a lot in the assessment of prepared catalysts. As a result of the cyclic photodegradation experiments, the decreasing photoactivity was valued as 80.57%. The regeneration experiment was carried out for further exploring the possibility of practical application. The comparison among the fresh photocatalyst, the cyclic photocatalyst and the regenerated one (named the Re-MFAA$_{10.5}$) was represented in **Fig. S6c**. The Re-MFAA$_{10.5}$ possessed a photodegradation efficiency of 88.13%, which is much higher than the cyclic photocatalyst. Concluded from the above information, the regeneration of this catalyst is feasible and may provide the prospect of a reduced cost of practical application.

Table S1 Kinetics parameters of zero-order, pseudo-first-order and second-order rate equations for every composite.

Sample	Zero-order		Pseudo-first-order		Second-order	
	k_0 [min^{-1}]	R^2	k_1 [min^{-1}]	R^2	k_2 [min^{-1}]	R^2
MIL-53(Fe)	0.00504	0.99345	0.00388	0.98134	0.00905	0.99345
Ag_3PO_4	0.00491	0.98708	0.00381	0.99182	0.00493	0.98708
Ag/Ag_3PO_4	0.01161	0.97905	0.00708	0.94824	0.01167	0.97905
$MFAA_{10.1}$	0.05341	0.8798	0.0186	0.99693	0.06817	0.8798
$MFAA_{10.5}$	0.07148	0.88693	0.02113	0.98902	0.10311	0.88693
$MFAA_{10.10}$	0.01747	0.99188	0.01087	0.84619	0.02489	0.99188

Fig. S1

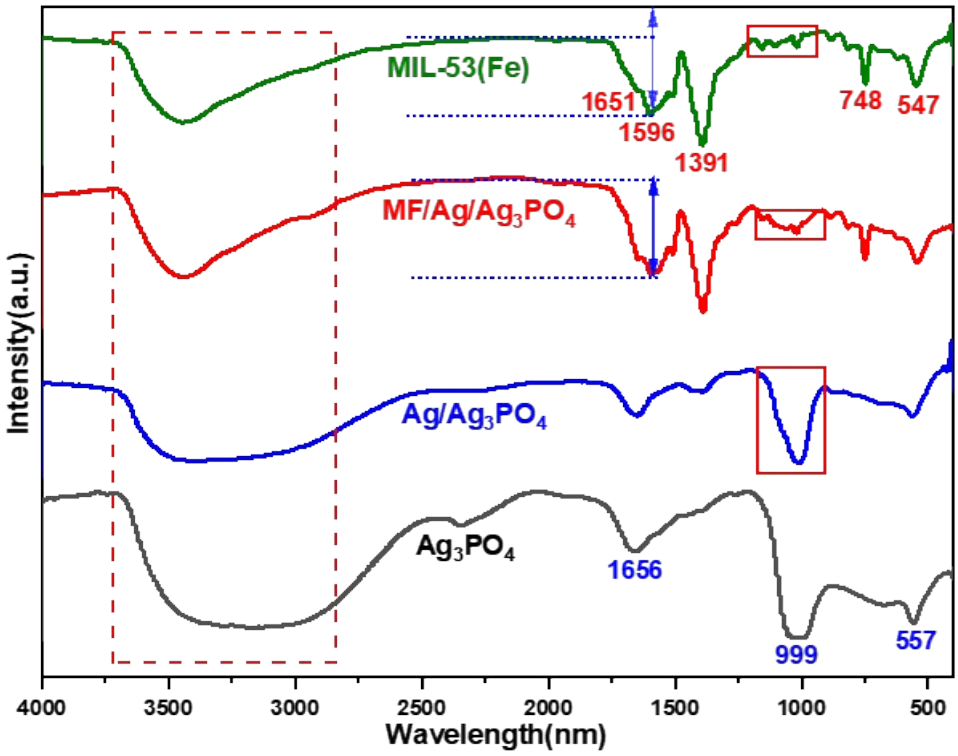

Fig. S1 FT-IR spectra of as-prepared composites

Fig. S2

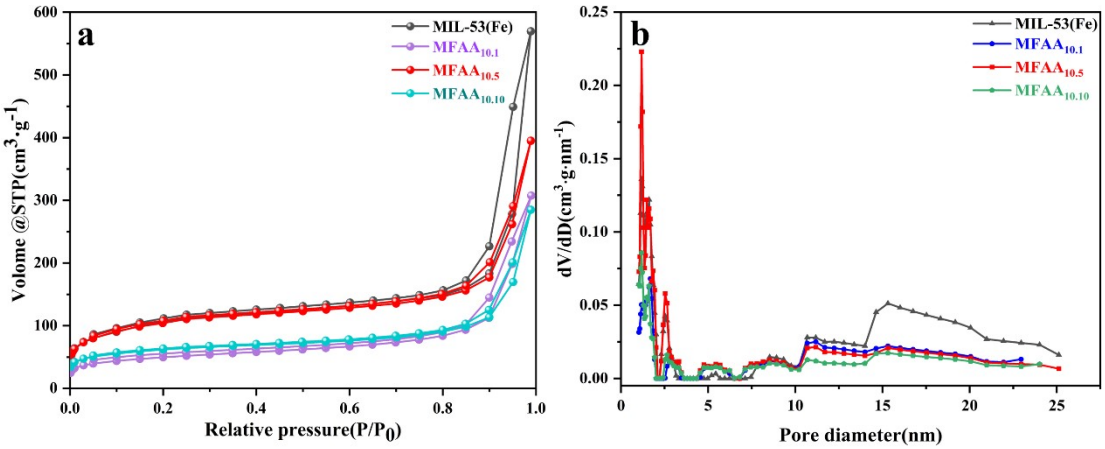

Fig. S2 (a) N_2 adsorption-desorption isotherm of MIL-53(Fe) and $MFAA_{10.x}$ composites and (b) BJH pore size distributions pattern of MIL-53(Fe) and $MFAA_{10.x}$

Fig. S3

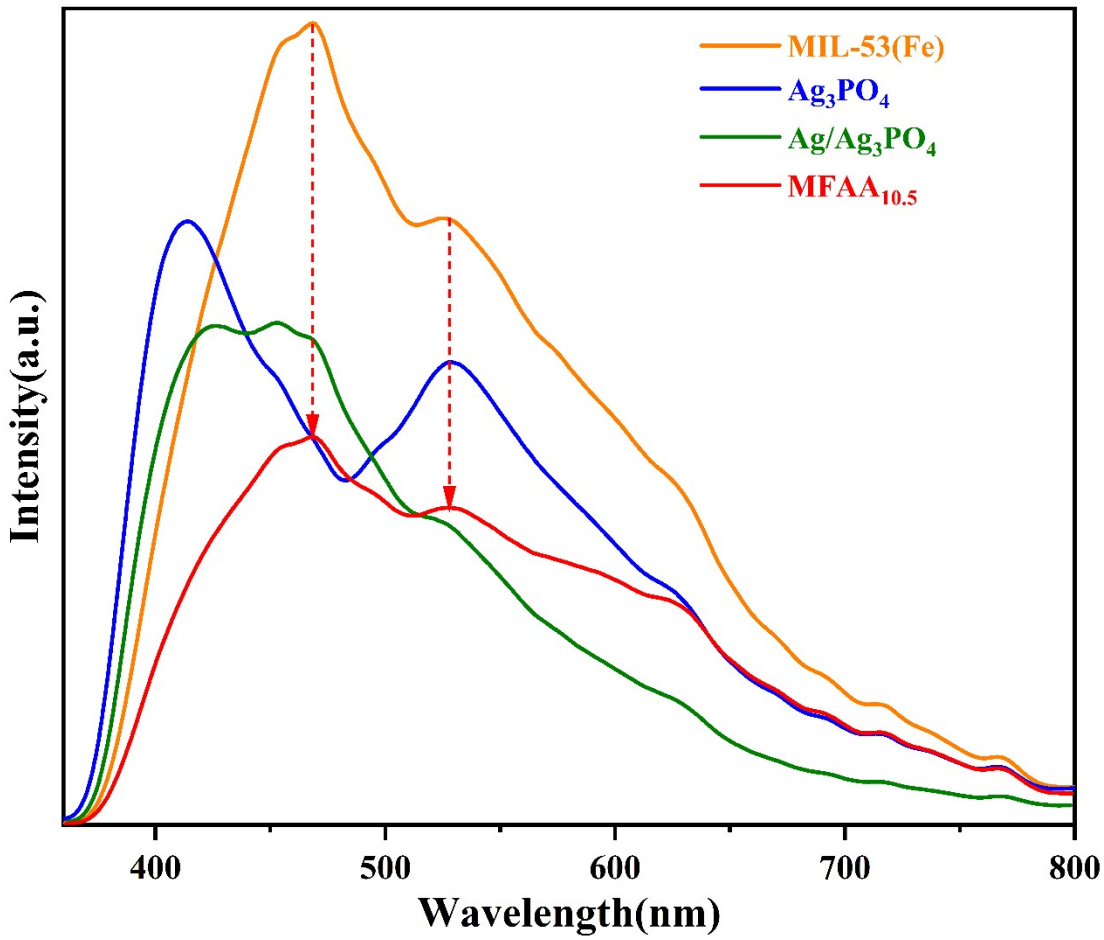

Fig. S3 PL spectra of the MIL-53(Fe), Ag_3PO_4, Ag/Ag_3PO_4 and $MFAA_{10.5}$ composites

Fig. S4

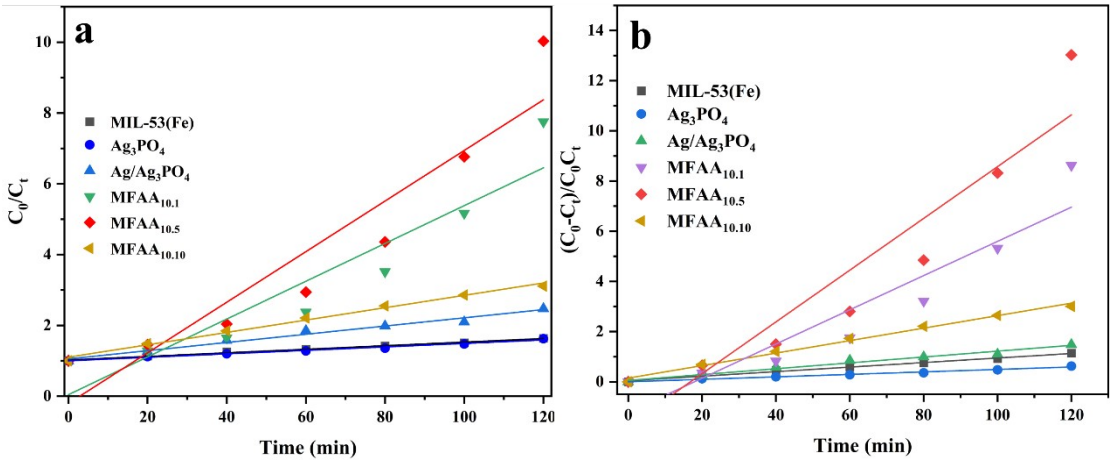

Fig. S4 The kinetic fitting curves of (a) zero-order and (b) second-order

Fig. S5

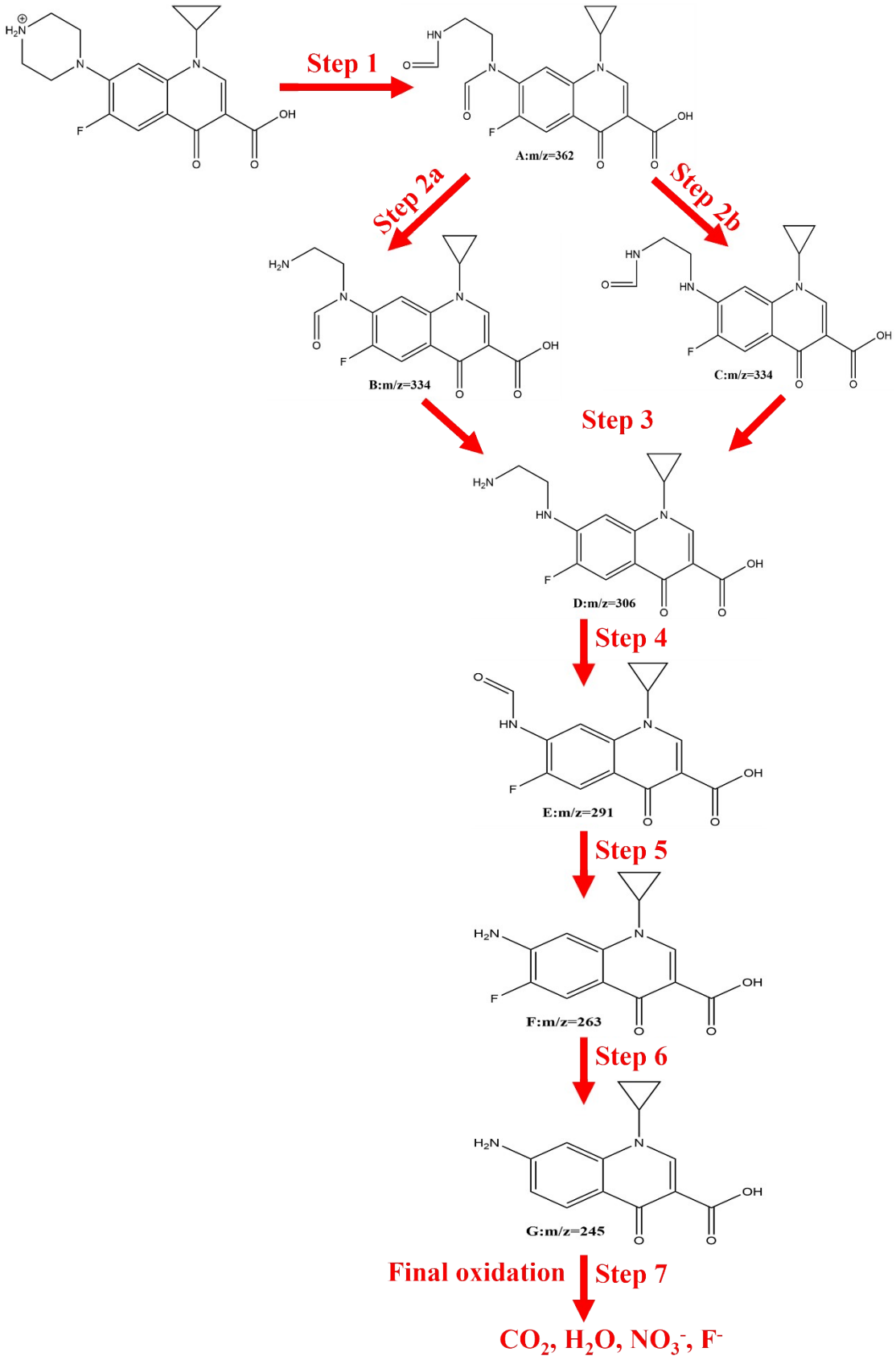

Fig. S5 The possible CIP photodegradation pathway

Fig. S6

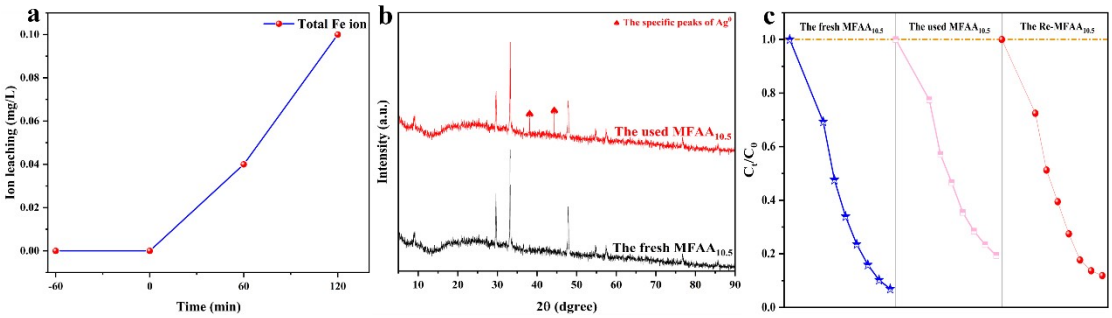

Fig. S6 (a) The concentration of the total Fe ions leaching during the photodegradation process (b) The XRD characterization of the used photocatalyst and the fresh one (c) The photoactivity of regeneration $MFAA_{10.5}$

Fig. S7

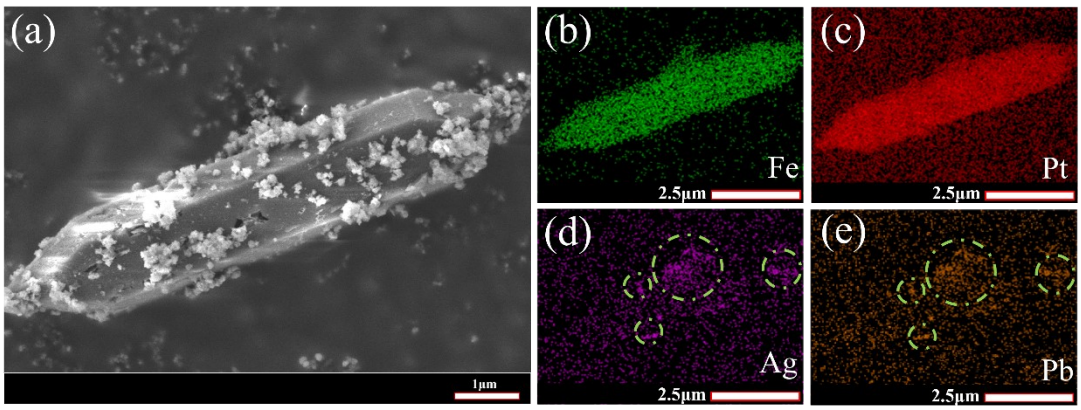

Fig. S7 (a) The SEM image of photo-deposed $MFAA_{10.5}$ composite and the EDX mapping images of (b) Fe, (c) Pt, (d) Ag and (e) Pb elements in photo-deposed $MFAA_{10.5}$ composite

Reference:

1. Y. Tu, L. Q. Ling, Q. W. Li, X. Y. Long, N. Liu and Z. Q. Li, *Opt. Mater.*, 2020, **110**, 110500.
2. G. Pandey, M. Tharmavaram, G. Phadke, D. Rawtani, M. Ranjan and K. P. Sooraj, *Sep. Purif. Technol.*, 2022, **293**, 121141.
3. S. T. He, T. F. Li, L. Zhang, X. F. Zhang, Z. W. Liu, Y. Zhang, J. Z. Wang, H. Z. Jia, T. C. Wang and L. Y. Zhu, *Chem. Eng. J.*, 2021, **424**, 254-264.
4. N. Liu, W. Y. Huang, M. Q. Tang, C. C. Yin, B. Gao, Z. M. Li, L. Tang, J. Q. Lei, L. F. Cui and X. D. Zhang, *Chem. Eng. J.*, 2019, **359**, 254-264.
5. X. J. Wen, C. G. Niu, L. Zhang, C. Liang, H. Guo and G. M. Zeng, *J. Catal.*, 2018, **358**, 141-154.